^{9}Be($\vec{p}$,d)^{8}Be and ^{9}Be($\vec{p}$,α)^{6}Li reactions at low energies

C. R. Brune, W. H. Geist, H. J. Karwowski, E. J. Ludwig, and K. D. Veal
Department of Physics and Astronomy, University of North Carolina at Chapel Hill, Chapel Hill, North Carolina 27599-3255
and Triangle Universities Nuclear Laboratory, Durham, North Carolina 27708-0308
(Received 17 October 1997)

Angular distributions of cross section and vector analyzing power have been measured for the ^{9}Be($\vec{p}$,d)^{8}Be and ^{9}Be($\vec{p}$,α)^{6}Li reactions for $77 \leqslant E_p \leqslant 321$ keV. Previous work has suggested that the low-energy cross section is enhanced by the $E_x = 6.57$ MeV subthreshold level in ^{10}B. The analyzing power measurements are particularly sensitive to the presence of the subthreshold level, leading to a definitive test of the hypothesis. The data are analyzed in terms of R-matrix and direct reaction calculations. We find that the magnitude and angular distribution of the ^{9}Be(p,d)^{8}Be reaction at very low energies can be explained by the direct reaction mechanism without any contribution from the subthreshold resonance. The implications of these results for the stellar reaction rate of the ^{9}Be(p,d)^{8}Be and ^{9}Be(p,α)^{6}Li reactions are discussed. [S0556-2813(98)06406-1]

PACS number(s): 26.35.+c, 24.50.+q, 24.70.+s, 27.20.+n

I. INTRODUCTION

The Be abundance in low-metallicity stars is an important probe of cosmic-ray and big-bang nucleosynthesis [1]. The abundances observed in these and other types of stars also provide important tests of galactic evolution and stellar structure models [2]. Beryllium has been observed at the level of $10^{-13} \lesssim n(^9\mathrm{Be})/n(\mathrm{H}) \lesssim 10^{-10}$ in many stars, a level consistent with models in which ^{9}Be is produced via collisions of p and α cosmic rays with CNO nuclei [3]. Furthermore, it has been established that the Be abundance observed in some stars is more than an order of magnitude lower than that seen in other stars expected to have the same quantity of Be produced by cosmic rays. This observation is taken to be evidence for Be depletion by thermonuclear reactions [1]. As discussed in Refs. [4,5], Be depletion mechanisms must be well understood in order to differentiate between cosmic-ray and big-bang production models. The depletion of Be results from the mixing of material from the stellar surface with material from interior regions where the temperature is sufficient for the ^{9}Be(p,d)^{8}Be and ^{9}Be(p,α)^{6}Li reactions to be effective ($\gtrsim 3.5\times10^6$ K). Thus, in order to make quantitative calculations of the ^{9}Be depletion, the cross sections for these reactions must be known at stellar energies.

In addition, the ^{9}Be(p,d)^{8}Be and ^{9}Be(p,α)^{6}Li reactions are important for determining the amount of ^{9}Be produced by primordial nucleosynthesis. While the standard big-bang model [6] predicts very little ^{9}Be production [$n(^9\mathrm{Be})/n(\mathrm{H}) \sim 10^{-18}$], some big-bang models which include baryon inhomogeneities predict significantly greater ^{9}Be production [7,8], possibly at a level observable with present technology, $n(^9\mathrm{Be})/n(\mathrm{H}) \sim 10^{-13}$.

Finally, we note that these reactions may have applications in advanced fusion reactors, such as discussed in Refs. [9,10].

A previous measurement [11] of the ^{9}Be(p,d)^{8}Be ($Q = 0.56$ MeV) and ^{9}Be(p,α)^{6}Li ($Q = 2.13$ MeV) reactions found the low-energy cross section in both reaction channels to be dominated by a broad ($\Gamma_{\mathrm{c.m.}} \approx 120$ keV) s-wave $J^\pi = 1^-$ resonance at $E_p = 330$ keV. At energies below the 1^- resonance, the angular distribution of deuterons was observed to be highly anisotropic about $\theta_{\mathrm{c.m.}} = 90°$. In order to explain this anisotropy, a significant but very uncertain contribution to the cross section was attributed to an opposite-parity subthreshold state. This uncertainty is reflected in the estimated $S(0)$ value (summed over both reaction channels) of 35^{+45}_{-15} MeV b [11]. The $S(0)$ value essentially determines the reaction rate, as the effective energy for this reaction at stellar temperatures is ~ 7 keV. The existence of a state at 6.57-MeV excitation in ^{10}B (20 keV below the ^{9}Be+p threshold) has been established by many experiments, but spin and parity determinations have not been in good agreement.

The high-intensity low-energy polarized proton beam available at Triangle Universities Nuclear Laboratory makes it possible to test the assumed reaction mechanism. The analyzing power for reactions induced by polarized protons incident on ^{9}Be is predicted to be large, if the subthreshold state has positive parity, and makes a significant contribution to the total cross section (i.e., if the previously reported analysis [11] is correct).

This paper describes measurements of the angular distributions of cross section and vector analyzing power for the ^{9}Be(p,d)^{8}Be and ^{9}Be(p,α)^{6}Li reactions. The data are analyzed in terms of R-matrix and direct reaction models. The implications of these results for the ^{9}Be(p,d)^{8}Be and ^{9}Be(p,α)^{6}Li thermonuclear reaction rates are discussed.

II. EXPERIMENTAL PROCEDURES

Measurements of the angular distributions of cross section and vector analyzing power for the ^{9}Be($\vec{p}$,d)^{8}Be and ^{9}Be($\vec{p}$,α)^{6}Li reactions were carried out using the low-energy beam facility at the Triangle Universities Nuclear Laboratory, as described below.

A. Beam

Beams of 80-keV polarized and unpolarized $^1\mathrm{H}^-$ and $^1\mathrm{H}^+$ ions were produced by an atomic-beam-polarized ion

source [12]. For on-target proton energies greater than 80 keV, the $^1H^-$ beam from the source was directed to the minitandem accelerator [13], where it was accelerated to the positive terminal potential, underwent charge exchange in a ~ 2-μg/cm^2 carbon foil, and was then further accelerated as $^1H^+$. For the on-target energy of 80 keV, the more-intense $^1H^+$ beam from the source was used, the charge exchange foil was rotated out of the beam, and the minitandem accelerator was grounded, so that the beam was transported through without further acceleration. Following the minitandem, the beam was magnetically analyzed and directed into the 107-cm-diam scattering chamber [14]. Beam currents on target varied between 10 nA and 3 μA, depending on detector count-rate requirements. For measurements with $E_p > 80$ keV, the energy calibration of the beam has been established to ± 1 keV, using the 240.0- and 340.5-keV resonances in $^{19}F(p,\alpha\gamma)$ and the 405.4- and 445.8-keV resonances in $^{27}Al(p,\gamma)$. The resonance energies were taken from Ref. [15].

For the polarized-proton-beam measurements with $E_p > 80$ keV, the beam polarization was determined using the $^6Li(\vec{p},^3He)^4He$ reaction in a polarimeter at the rear of the 107-cm-diam scattering chamber as described in Ref. [16]. For these measurements, the beam energy was set to give a mean proton energy of 321 keV, where the polarimeter is well calibrated. The polarization of the $^1H^+$ beam used for the $E_p = 80$ keV measurements was assumed to be the same as that determined for the $^1H^-$ beam before and after the positive beam measurements. The systematic error in the beam polarization is estimated to be $\pm 5\%$, except for the $E_p = 80$ keV measurement, for which we estimate $\pm 7\%$.

A Wien filter downstream from the ion source was set so that the spin-quantization axis was vertical in the laboratory, perpendicular to the scattering plane. The polarized-beam data were taken with two spin states, with polarizations p_1 (≈ 0.7) and p_2 (≈ -0.7). The desired hyperfine states of atomic hydrogen were cycled approximately every second. This technique minimizes the effects of slow changes in beam position, target thickness, or amplifier gain on the measured analyzing powers.

B. Targets and detectors

The targets consisted of 10 μg/cm^2 of ^{9}Be evaporated on 5-μg/cm^2 carbon foils. The foils were supported on a steel frame with a 0.8-cm-diam hole and positioned in the center of the scattering chamber. The proton beam lost between 6 and 10 keV in the ^{9}Be layer; the results reported here are for the mean proton energy in the target. The beam was collimated to produce a 0.4 cm $\times$ 0.4 cm spot on the target.

The reaction products were detected using 100-μm-thick Si surface barrier detectors. Sets of three detectors separated by 20° were placed on each side of the beam in the chamber; each detector subtended a solid angle of ≈ 5 msr. For most of the measurements, the detectors were covered with 0.9-μm Ni or 2-μm Mylar foils to stop or degrade the energy of the elastically scattered protons. A sample spectrum is shown in Fig. 1. In some instances, no foils were used on the detectors at backward angles, in order to allow ^{6}Li ions from the $^9Be(p,\alpha)^6Li$ reaction to be detected. For measurements with $70° \leq \theta_{lab} \leq 110°$ the targets were rotated to 45° with respect to the beam. In these cases, the beam loses 40% more energy in the target, leading to slightly lower mean energy (no corrections were made for this effect, as it is estimated to be negligible). Pulsers were inserted into the detector spectra to facilitate dead-time corrections, which were less than 5% in all measurements.

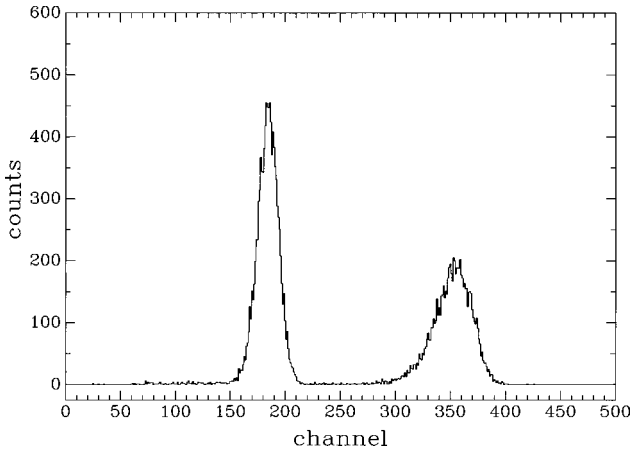

FIG. 1. Charged-particle spectrum obtained at $\theta_{lab} = 150°$, with a mean proton energy in the target of 197 keV. The deuteron and α-particle peaks are centered at channels 185 and 360, respectively.

C. Measurements

Measurements of the angular distributions of cross section and vector analyzing power were carried out for seven different incident energies, corresponding to mean proton energies in the target of 77, 147, 172, 197, 247, 297, and 321 keV.

The measurements of the angular distribution of the cross section were carried out an using unpolarized beam. One set of detectors was used as a monitor, and was placed at laboratory angles of 130°, 150°, and 170°. The other set of detectors was mounted on a movable plate and covered the angular range of $15° \leq \theta_{lab} \leq 170°$ in 10° steps (a 5° step was used at far-forward angles).

The majority of the analyzing power measurements were carried out with two sets of three detectors, with each set placed symmetrically on either side of the beam. The measurements covered $15° \leq \theta_{lab} \leq 165°$ in $5°-15°$ steps.

III. RESULTS

A. Cross section measurements

The normalized yields of deuterons and α particles were calculated using

$$W = F_i \frac{N_d}{N_{mon}}, \tag{1}$$

where N_d is the number of counts in the moving detector, N_{mon} is the sum of deuteron and α-particle counts in the 150° and 170° monitor detectors (the 130° monitor was blocked when the target was rotated 45°), and the F_i factors correct for the slightly different solid angles subtended by each detector. Both N_d and N_{mon} were corrected for dead-time effects. The F_i factors for each detector were deter-

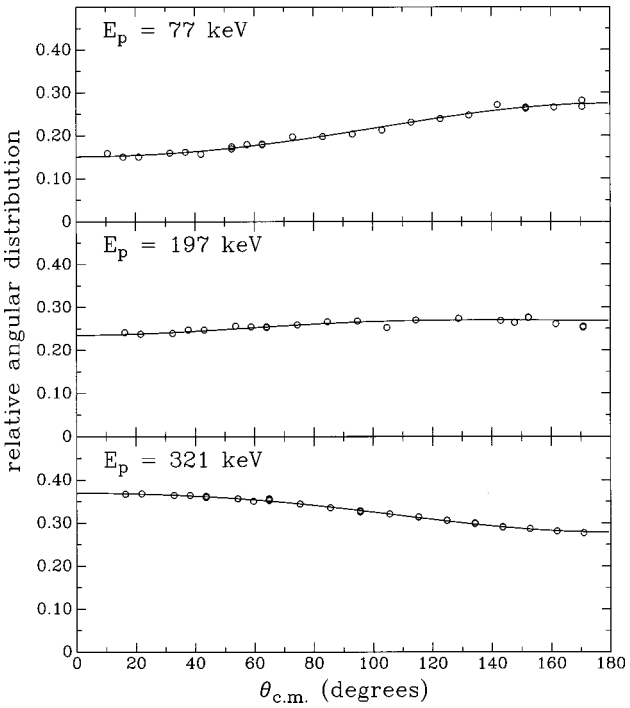

FIG. 2. Sample cross section angular distributions for the ^{9}Be(p,d)^{8}Be reaction. The experimental data are shown as circles and the Legendre polynomial fits are given by the solid lines. If not shown, the error bars are smaller than the data points.

mined by comparing the yields at overlapping angles. The results were converted to the center-of-mass system, and are shown in Figs. 2 and 3, renormalized as described below.

The cross section can be expanded in terms of Legendre polynomials $P_l(\cos\,\theta_{c.m.})$ using

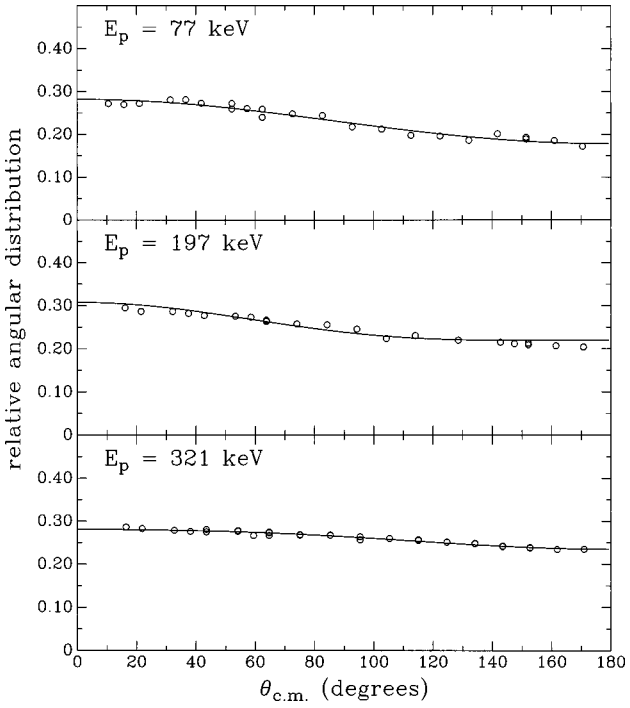

FIG. 3. Sample cross section angular distributions for the ^{9}Be(p,α)^{6}Li reaction. The experimental data are shown as circles and the Legendre polynomial fits are given by the solid lines. If not shown, the error bars are smaller than the data points.

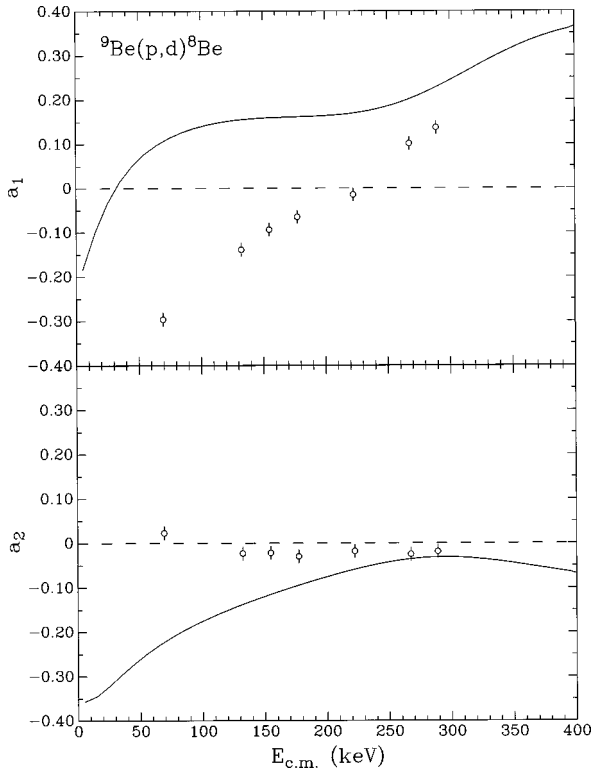

FIG. 4. The fitted a_l coefficients for the ^{9}Be(p,d)^{8}Be reaction (circles) and the R-matrix parametrization of Ref. [11] (solid lines).

$$W(\theta_{c.m.}) = N_W\left[1+\sum_{l=1}^{N_a} a_l P_l(\cos\,\theta_{c.m.})\right], \tag{2}$$

where N_W is an overall normalization factor and N_a is the number of terms in the sum. The data were fit to Eq. (2) using $N_a=2$, as this assumption was sufficient to obtain an excellent fit to the data. When the angular distribution data were fitted with $N_a=3$, the fitted a_3 coefficients were not statistically different from zero. The angular distribution data and fits, renormalized so that $N_W=1$, are shown in Figs. 2 and 3. The fitted a_l coefficients are shown in Figs. 4 and 5.

B. Analyzing power measurements

The analyzing power measurements were taken using two spin states with polarizations p_1 and p_2. The analyzing powers A_y were determined from the measured yields using

$$A_y = -\frac{R-1}{p_1 - Rp_2} \tag{3}$$

for the right detectors and

$$A_y = \frac{L-1}{p_1 - Lp_2} \tag{4}$$

for the left detectors, where $R = Y_R^1/Y_R^2$, $L = Y_L^1/Y_L^2$, and Y_R^i and Y_L^i are the yields of detected particles for spin state i in the right and left detectors, respectively. The yields were corrected for dead time and normalized by the number of incident particles (determined by beam-current integration). The values for A_y found from the right and left detectors

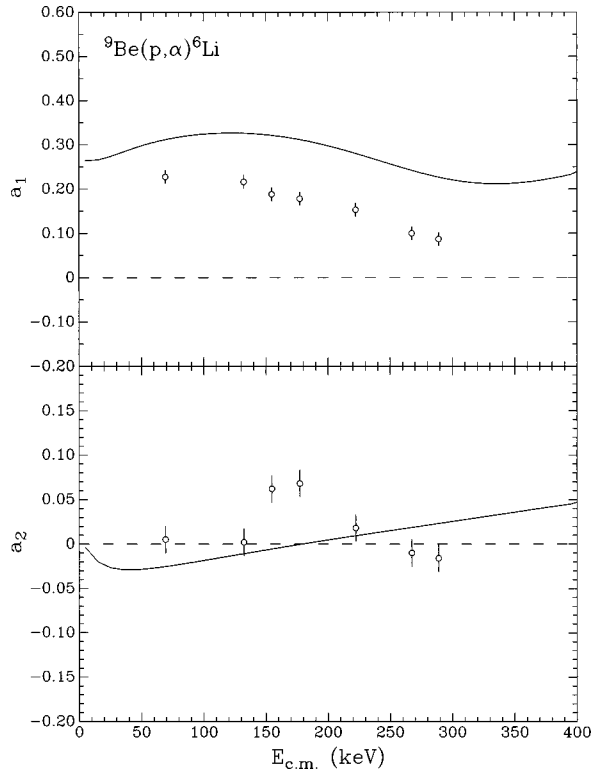

FIG. 5. The fitted a_l coefficients for the ^{9}Be$(p,\alpha)^6$Li reaction (circles) and the R-matrix parametrization of Ref. [11] (solid lines).

were identical within statistical errors, and an average weighted by the statistical errors was used to determine the final A_y values. The analyzing powers determined from the detected ^{6}Li particles were converted to the α-particle coordinate system by reversing the sign of the analyzing power and replacing $\theta_{\text{c.m.}}$ by $180°-\theta_{\text{c.m.}}$. The resulting A_y values are shown in Figs. 6 and 7.

The expansion for the angular dependence of the analyzing power is given by [17]

$$A_y=\frac{\Sigma_{l=1}^{N_b} b_l P_l^1(\cos\ \theta_{\text{c.m.}})}{1+\Sigma_{l=1}^{N_a} a_l P_l(\cos\ \theta_{\text{c.m.}})}, \tag{5}$$

where the a_l coefficients and N_a are the same as in Eq. (2), the associated Legendre polynomials $P_l^1(\cos\theta)$ are defined in Ref. [18], and N_b is the number of associated Legendre polynomial terms included in the sum. The required a_l coefficients were taken from the fits to the unpolarized angular distribution data (Sec. III A). The data were fit to Eq. (5) using $N_b=3$ for the ^{9}Be$(p,d)^8$Be reaction and $N_b=2$ for the ^{9}Be$(p,\alpha)^6$Li reaction, as these assumptions were sufficient to obtain an excellent fit to the data. When the (p,α) data were fit using $N_b=3$, the fitted b_3 coefficients were not statistically different from zero. The analyzing power data and fits are shown in Figs. 6 and 7. The fitted b_l coefficients are shown in Figs. 8 and 9.

IV. ANALYSIS AND DISCUSSION

A. R-matrix calculations and the role of the $E_x=6.57$ MeV state

The low-energy cross section of the ^{9}Be$(p,d)^8$Be and ^{9}Be$(p,\alpha)^6$Li reactions will be significantly enhanced if the

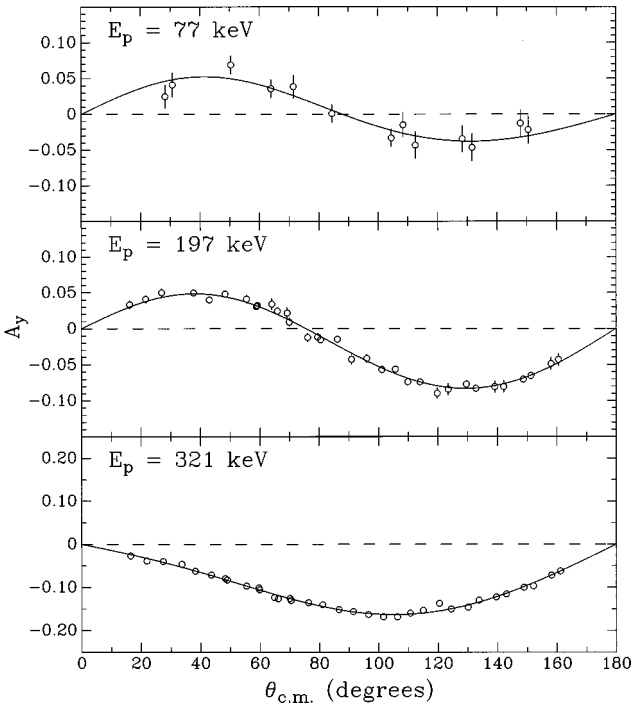

FIG. 6. Sample A_y distributions for the ^{9}Be$(\vec{p},d)^8$Be reaction. The experimental data are shown as circles and the Legendre polynomial fits are given by the solid lines.

subthreshold state at $E_x=6.57$ MeV has a spin and parity which allow the state to be populated by s or p waves in the ^{9}Be$+p$ channel, and if the reduced widths are sufficiently large. Given the excitation energy and total width of this state, its contribution to the total cross section will be negligible if $l_p\geq 2$ in the entrance channel, even for reduced pro-

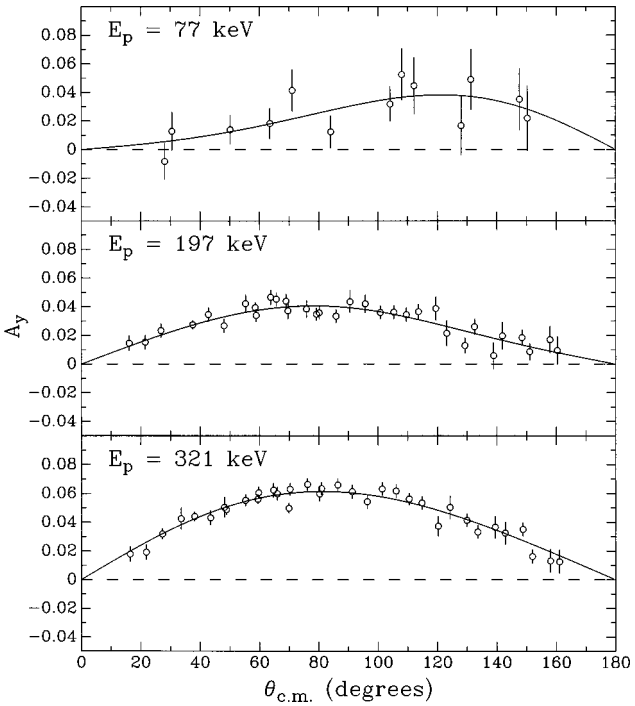

FIG. 7. Sample A_y distributions for the ^{9}Be$(\vec{p},\alpha)^6$Li reaction. The experimental data are shown as circles and the Legendre polynomial fits are given by the solid lines.

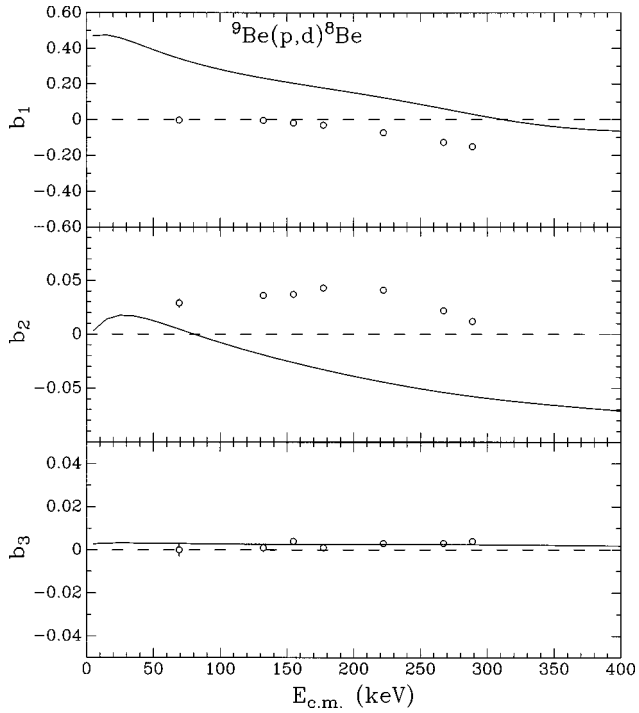

FIG. 8. The fitted analyzing power coefficients b_l for the ^{9}Be($\vec{p}$,d)^{8}Be reaction (circles) and the R-matrix parametrization of Ref. [11] (solid lines). If not shown, the errors bars are smaller than the data points.

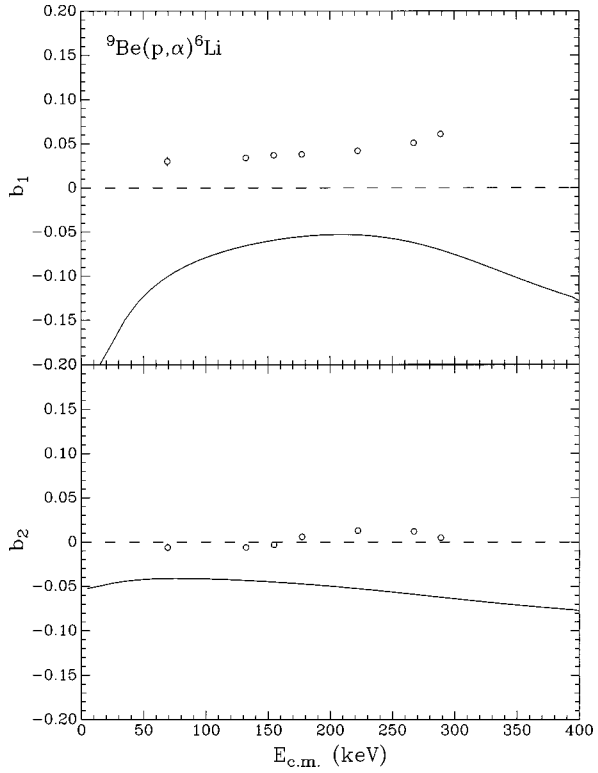

FIG. 9. The fitted analyzing power coefficients b_l for the ^{9}Be($\vec{p}$,α)^{6}Li reaction (circles) and the R-matrix parametrization of Ref. [11] (solid lines). If not shown, the error bars are smaller than the data points.

TABLE I. Existing results for the spin and parity of the $E_x = 6.57$ MeV level of ^{10}B. Results from proton transfer reactions on ^{9}Be provide information on l_p, the orbital angular momentum of the transferred proton. Results reported as tentative are indicated with parentheses.

Reaction	Results	Reference
^{9}Be(p,d) and ^{9}Be(p,α)	$\pi = +$	[11]
^{6}Li(α,α)	$l_\alpha = 3$ ($J^\pi = 2^-$ or 4^-)	[19]
^{6}Li(α,α)	$l_\alpha = 3$ ($J^\pi = 2^-$ or 4^-)	[20]
^{11}B(^{3}He,α)^{10}B(α_0)^{6}Li	$J \geq 3$, ($J^\pi = 3^-$ or 4^-)	[22]
^{10}B(n,n')	$\pi = -$	[38]
^{10}B(p,p')	$\pi = -$	[39]
^{9}Be(d,n)	$l_p = 1$	[40]
^{9}Be(d,n)	($l_p = 3$)	[41]
^{9}Be(d,n)	$l_p = 1$ or 2	[42]
^{9}Be(^{3}He,d)	($l_p = 1$)	[43]
^{9}Be(^{3}He,d)	($l_p = 2$)	[21]

ton widths up to the single-particle limit, due to angular-momentum barrier considerations. In the work of Sierk and Tombrello [11], this state was assumed to have positive parity, and therefore could be formed by p waves in the entrance channel. The observed anisotropy in the low-energy ^{9}Be(p,d)^{8}Be cross section angular distribution could then be explained by the presence of interfering s- and p-wave amplitudes.

There have been many other measurements of the spectroscopic properties of the $E_x = 6.57$ MeV state of ^{10}B; unfortunately, as shown in Table I, there are a wide variety of spin and parity assignments. In addition to spin and parity determinations, the two measurements of ^{6}Li(α,α) scattering have consistently determined the total width: $\Gamma_{c.m.} = 25.1 \pm 1.1$ [19] and $\Gamma_{c.m.} = 26 \pm 3$ [20]. It is important to note that the total width of this state provides some useful constraints on the assumed reduced α-particle and deuteron widths.

In the relatively recent study of proton transfer reactions by Bland and Fortune [21], the authors attempt to fit ^{9}Be(^{3}He,d) and ^{9}Be(d,n) data using distorted-wave Born-approximation calculations. They note that neither the assumption of $l_p = 1$ or $l_p = 2$ for the transferred proton orbital angular momentum in populating the 6.57-MeV state provides a convincing fit to the data. However, the requirement that the spectroscopic strength observed in the two reactions should be self-consistent induced the authors to favor $l_p = 2$.

An analysis of α-α angular correlations from ^{11}B(^{3}He,α)^{10}B(α_0)^{6}Li determined $J \geq 3$ from the complexity of the angular dependence of the correlation [22]. In addition, the parity was tentatively determined to be negative. These results, if correct, would have important consequences for the ^{9}Be$+p$ reactions, as $J \geq 3$ rules out s-wave formation in the entrance channel, and negative parity rules out p-wave formation.

The measurements of ^{6}Li(α,α) scattering [19,20] determined that the 6.57-MeV state is formed by $l = 3$ α particles, with $J^\pi = 2^-$ or 4^- favored on the basis of the quality of fits to the scattering data. These determinations of J must be considered tentative, due to the simple form assumed for the

nonresonant amplitudes and the neglect of the deuteron channel in the analyses.

Some further information on the spin and parity of this state is provided by the recent measurement of ^{10}B(e,e') [23]. It was found that the measured electromagnetic form factors for this state were well reproduced by shell-model calculations which assumed $J^\pi = 4^-$.

On the basis of these determinations, it seems most likely that the 6.57-MeV state has $J^\pi = 3^-$ or 4^-. This assumption is consistent with the majority of the results in Table I, and is only in conflict with the previous analysis of the ^{9}Be$(p,d)^8$Be and ^{9}Be$(p,\alpha)^6$Li reactions [11] and some of the early proton transfer analyses. However, due to the uncertain situation outlined above, a definitive determination of J^π for this state would be most welcome.

The only analysis of the ^{9}Be$(p,d)^8$Be and ^{9}Be$(p,\alpha)^6$Li reactions, however, assumed $\pi = +$ for the 6.57 MeV level. In Ref. [11], the total and differential cross sections for ^{9}Be$(p,d)^8$Be and ^{9}Be$(p,\alpha)^6$Li were fitted using an R-matrix parametrization which included the $E_x = 6.57$ MeV subthreshold state.

The dominant features in the ^{9}Be$(p,d)^8$Be and ^{9}Be$(p,\alpha)^6$Li cross section data below $E_{\text{c.m.}} = 400$ keV are effects due to the $J^\pi = 1^-$ level at $E_{\text{c.m.}} = 310$ keV. The asymmetry of the angular distribution about $\theta_{\text{c.m.}} = 90°$ and the nonzero analyzing power indicate the presence of $l_p = 1$ components in the ^{9}Be$(p,d)^8$Be reaction. Since a proton ($J^\pi = \frac{1}{2}^+$) and ^{9}Be ($J^\pi = \frac{3}{2}^-$) can couple to form five different J^π values with $l_p \leqslant 1$, it is not possible to uniquely determine the role of each component from the available data. The R-matrix formalism does, however, provide a convenient means for assessing the role of the subthreshold state. If this level is formed with $l_p = 1$ and contributes significantly to the total cross section, R-matrix theory unambiguously predicts that the differential cross section and analyzing power will show large interference effects as this level is approached at very low energies.

The R-matrix parameters found by Sierk and Tombrello [11] are given in Table II. The boundary-condition constants are chosen so that the level shift vanishes at the energy of the resonance for each spin and parity. R-matrix theory [24] describes the energy dependence of the scattering matrix elements. The total cross section and angular distribution coefficients are calculated from the scattering matrix elements using formulas given in Ref. [24]. The relationship between the analyzing power coefficients and the scattering matrix elements has been given by Welton [17]. Examples of R-matrix calculations of analyzing power coefficients are given in Refs. [25,26].

In Figs. 4, 5, 8, 9, and 10 we show the S factor, angular distribution coefficients, and analyzing power coefficients calculated from the R-matrix parameters given in Table II. Note in particular Fig. 8, which shows that the analyzing power coefficient b_1 for the ^{9}Be$(\vec{p},d)^8$Be reaction is predicted to be very large at low energies, in contrast to the experimental data. The angular distribution coefficients calculated in the present work are somewhat different than those given in Ref. [11]; the origin of the discrepancy is not understood.

TABLE II. The R-matrix parameters reported by Sierk and Tombrello [11,44]. The first two columns give the resonance energy and J^π values of the resonances. The remaining columns give the reaction channel, interaction radii a_c, orbital angular momentum l, the channel spin s, and the reduced width γ_c.

$E_{\text{c.m.}}$ (MeV)	J^π	Channel	a_c (fm)	l	s	γ_c (MeV)
		p	7.396	0	1	0.65
		p	7.396	2	1	0.50
0.310	1^-	p	7.396	2	2	0.51
		d	8.650	1	1	0.28
		α	7.954	1	1	0.15
		p	7.396	1	1	0.10
		p	7.396	3	1	0.10
−0.010	2^+	p	7.396	1	2	0.11
		p	7.396	3	2	0.11
		d	8.650	2	1	0.50
		α	7.954	2	1	−0.05
		p	7.396	1	1	0.60
		p	7.396	1	2	−0.61
		p	7.396	3	2	0.20
0.410	1^+	d	8.650	0	1	0.40
		d	8.650	2	1	1.00
		α	7.954	0	1	0.20
		α	7.954	2	1	0.01

A new analysis has been performed, in order to see if a new set of parameters could be found which simultaneously fits the cross section and analyzing power data. The three-level parametrization of Ref. [11] was used as a starting point. The resonance energy and reduced widths of the $J^\pi = 1^-$ level at $E_{\text{c.m.}} = 310$ keV are well determined (except for the signs of the reduced widths) by the energy dependence and magnitude of the ^{9}Be$(p,d)^8$Be and ^{9}Be$(p,\alpha)^6$Li cross sections near this resonance, and so the previously assumed parameters were used for this level. The properties of the higher-energy resonance at $E_{\text{c.m.}} = 410$ keV were found to have a rather minor effect on the cross section and analyzing

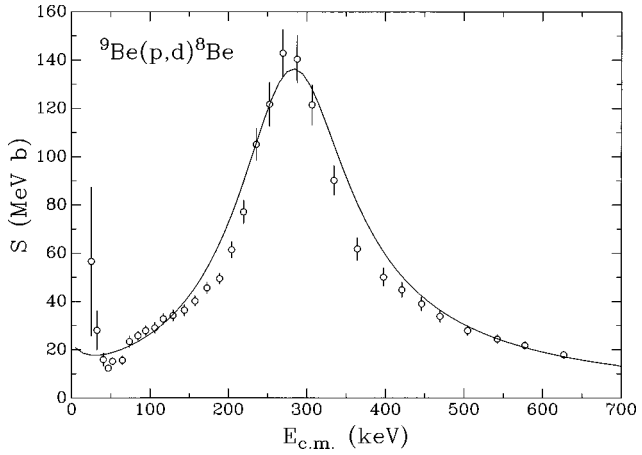

FIG. 10. The ^{9}Be$(p,d)^8$Be S-factor data [11] (circles), compared to to the calculation using the R-matrix parametrization of Ref. [11] (solid line).

power at very low energies, and so these parameters were not varied during the analysis. In addition, the $l_p=2$ and $l_p=3$ reduced proton widths from Ref. [11] were left unchanged for the same reason. This analysis differs from that of Sierk and Tombrello [11] by the inclusion of analyzing power data, which places additional constraints on the reaction amplitudes. The analysis was carried out using different values for the spin and parity of the 6.57-MeV level consistent with $l_p=1$, as well as all possible combinations of signs for the reduced widths of the 310-keV level. The $l_p=1$ reduced proton widths and the reduced deuterons and alpha widths of the subthreshold level were varied, subject to the constraint that total width of this level be 26 keV. In agreement with Ref. [11], we found that it was possible to obtain a reasonable description of the total cross section and angular distribution coefficients for several different parameter sets. However, it was not possible to also fit the analyzing power data with these three-level parametrizations. We found that when the parameters were adjusted to fit the anisotropy in low-energy angular distribution coefficients (primarily a_1), the predicted analyzing power was very large, in contrast to the experimental data ($A_y<0.1$ at the lowest energies). If the parity 6.57-MeV level is allowed to be negative, it is not possible to describe either the cross section angular distribution or analyzing power data. We are thus led to conclude that the anisotropy in the low-energy angular distribution is *not* due to interference effects from the 6.57-MeV level.

B. Direct-reaction calculations

There have been several recent calculations which use the direct-reaction framework to describe low-energy proton-induced nuclear reactions. Direct-reaction studies of cross section data only have been published for ^{7}Li(p,α)^{4}He [27,28], ^{11}B(p,α_0)^{8}Be [29], and ^{19}F(p,α_0)^{16}O [30]. These nonresonant reactions appear to have been successfully described using direct-reaction models. The predictive power of these models is not clear, however, since in general the results are quite sensitive to the adopted optical potentials and spectroscopic factors. Another difficulty with the direct-reaction models is the inclusion of resonant contributions to the reaction mechanism. In spite of these limitations, these models appear to correctly describe the reaction mechanism in certain cases, and are particularly useful for extrapolating the measured cross sections to the extremely low energies needed in astrophysical applications.

We have investigated the possibility that the direct-reaction mechanism is making a significant contribution to the ^{9}Be(p,d)^{8}Be cross section below the $E_p=330$ keV resonance. This mechanism is suggested by the large spectroscopic factor ($\mathcal{S}=1.13$) found previously [31] for the ^{8}Be $+n$ configuration in ^{9}Be. Furthermore, as a result of the small 560-keV Q value for this reaction, both the incoming and outgoing channels will be below the Coulomb barrier for very low incident energies. As discussed in Ref. [32] the direct mechanism is selectively enhanced under these conditions. The presence of the weakly bound neutron ($E_B=1.67$ MeV) in ^{9}Be also favors the direct-pickup process at very low energies, since the incoming proton can react at larger radii where its wave function is less attenuated by the Coulomb barrier. It is also known that direct-transfer reactions where both the incoming and outgoing channels are below the Coulomb barrier give rise to angular distributions which are peaked at backward angles [32]. The direct-reaction mechanism may thus provide a natural explanation for the observed anisotropy in the ^{9}Be(p,d)^{8}Be differential cross section at low energies, without requiring the presence of an interfering subthreshold level. Another advantage of being below the Coulomb barrier is that the sensitivity to the optical potentials is minimized, as the scattering waves are primarily determined by the point-Coulomb potentials.

TABLE III. The adopted parameters for the ^{8}Be$+n$ bound state and the elastic-scattering potentials. The potentials are defined in terms of the parameters by Eq. (6).

System	V_R (MeV)	r_0 (fm)	a_0 (fm)	W_S (MeV)	r_I (fm)	a_I (fm)	r_C (fm)
^{8}Be$+n$	44.4	1.20	0.65	-	-	-	-
^{9}Be$+p$	55.0	1.24	0.63	13.0	1.36	0.35	1.3
^{8}Be$+d$	113.0	0.82	0.96	10.0	0.90	0.90	1.3

The distorted-wave Born-approximation (DWBA) calculations were carried out using the computer code PTOLEMY [33] which treats finite-range effects without approximation. The ^{8}Be$+n$ bound-state potential and the elastic-scattering potentials were taken to be of the form

$$V(r)=-\frac{V_R}{1+\exp[(r-R_0)/a_0]} - \frac{4iW_S\exp[(r-R_I)/a_I]}{\{1+\exp[(r-R_I)/a_I]\}^2}+V_C(r), \qquad (6)$$

where $R_0=r_0A^{1/3}$, $R_I=r_IA^{1/3}$, $V_C(r)$ is the Coulomb potential resulting from a uniformly charged sphere of radius $R_C=r_CA^{1/3}$, and A is the target mass number. The adopted parameters are given in Table III. The ^{9}Be$+p$ potential parameters were taken from Ref. [34], which fit the elastic scattering of protons by ^{9}Be at higher energies. For obvious reasons there are no data for the elastic scattering of deuterons by ^{8}Be; we used a potential found from fitting the elastic scattering of deuterons by ^{9}Be at higher energies [35]. The spin-orbit potentials were neglected, as they were found to have a minor influence on the calculated cross sections and analyzing powers. For the deuteron bound state, the Reid soft-core wave function [36] was used. The neutron bound-state parameters for ^{9}Be were taken from Ref. [31].

The calculated astrophysical S factor, angular distribution coefficients, and analyzing power coefficients for ^{9}Be(p,d)^{8}Be are shown by the solid curves in Figs. 11–13. The calculated S factor has been normalized by the spectroscopic factor $\mathcal{S}=1.13$ [31]. Also shown by the dashed curves is the calculation using only the point-Coulomb potential for the incoming and outgoing distorted waves. It is seen that the inclusion of the nuclear potential has a significant effect on the calculation. By varying the potential parameters, it was determined that the calculation is primarily sensitive to the real part of the nuclear potential in the ^{8}Be$+d$ channel. Apparently, as a result of the small positive Q value of the

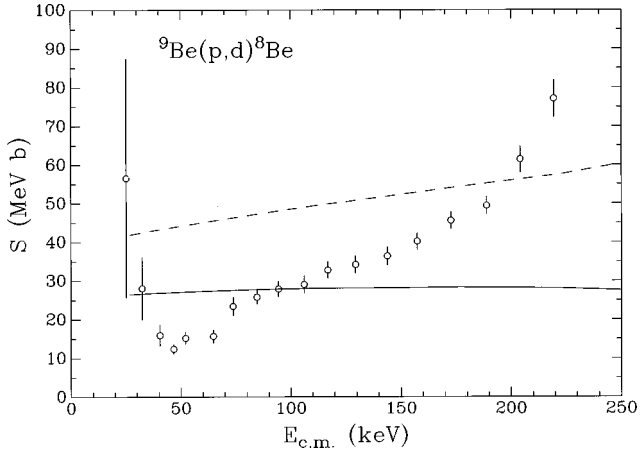

FIG. 11. S-factor data for the ^{9}Be$(p,d)^8$Be reaction [11], compared to the direct reaction calculations with the full optical potentials (solid line) and the calculations with only point-Coulomb potentials (dashed line).

reaction, the outgoing deuterons have sufficient energy compared to the Coulomb barrier to still be sensitive to the nuclear potential.

As seen in Figs. 11–13, the full calculation including the nuclear potentials gives a fair description of the S factor and a good description of the cross section angular distribution and analyzing power coefficients at the lowest energies. The poorer agreement with the S factor is clearly due to the neglect of the $E_p = 330$ keV resonance, as the elastic-scattering

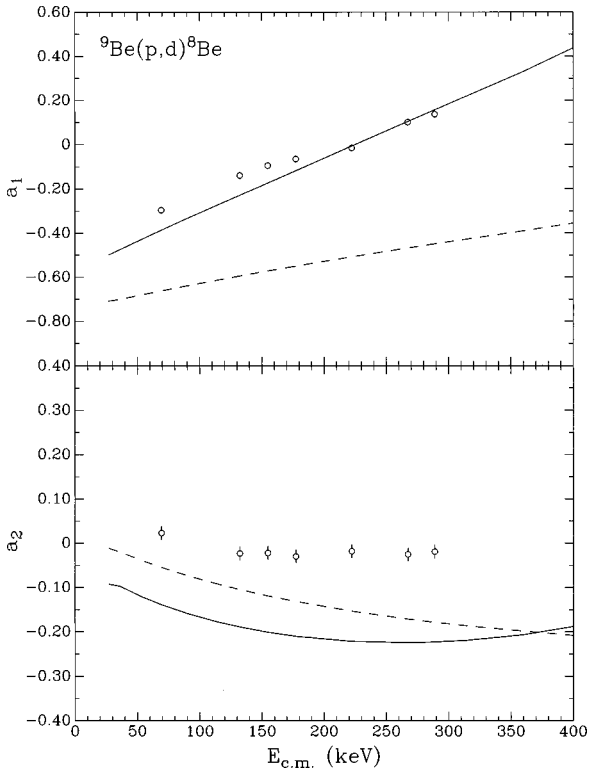

FIG. 12. The experimental ^{9}Be$(p,d)^8$Be a_l coefficients (circles), compared to the direct reaction calculations with the full optical potentials (solid line) and the calculations with only point-Coulomb potentials (dashed line). If not shown, the error bars are smaller than the data points.

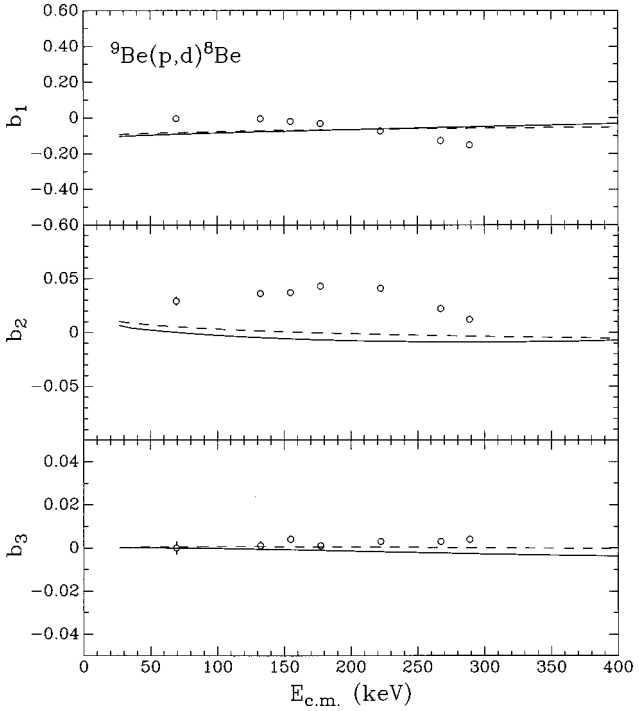

FIG. 13. The experimental ^{9}Be$(p,d)^8$Be b_l coefficients (circles), compared to the direct reaction calculations with the full optical potentials (solid line) and the calculations with only point-Coulomb potentials (dashed line). If not shown, the error bars are smaller than the data points.

potentials used in the DWBA calculation do not give rise to any resonances in this energy range. The calculations predict the backward peaking of the cross section angular distributions (or large negative a_1 coefficient), in agreement with the experimental data at the lowest energies. The small magnitude of the calculated analyzing power coefficients is in general agreement with the data, although they do not agree in detail. The inclusion of spin-orbit forces with strengths determined from higher-energy elastic scattering [34,35] does not significantly change the calculated analyzing power. We conclude that the discrepancy in the analyzing power coefficient is most likely due to a small amplitude from a distant state which is not included in the DWBA calculation. The calculations show that the direct-reaction mechanism is very important at low energies. These findings differ from those reported in Ref. [11], which indicated that the direct-reaction contribution to the cross section was negligible. Since the ^{9}Be$(p,\alpha)^6$Li reaction is well described by the previous R-matrix parametrization [11], and the direct-reaction mechanism is expected to be less important for this reaction, no direct reaction calculations have been attempted for this reaction.

V. CONCLUSIONS

We have measured angular distributions and analyzing powers for the ^{9}Be$(p,d)^8$Be and ^{9}Be$(p,\alpha)^6$Li reactions for seven energies with $77 \leqslant E_p \leqslant 321$ keV. A previous analysis of total and differential cross section data [11] found that the observed anisotropy in the ^{9}Be$(p,d)^8$Be differential cross section could be explained by interference with a positive-

parity subthreshold level at 6.57-MeV excitation in ^{10}B. A survey of existing results for the spin and parity of the 6.57-MeV level of ^{10}B indicates that this level most likely has negative parity, although there exists no definitive determination. Extending the R-matrix analysis of Ref. [11] to include the analyzing power data measured in this experiment, we conclude that it is not possible to explain the anisotropy in the differential cross section by assuming interference from the subthreshold level. The data obtained using the polarized proton beam were critical in reaching this conclusion, as the previous analysis [11] based on unpolarized data could not determine the role of the subthreshold state. We also carried out direct-reaction calculations for the ^{9}Be(p,d)^{8}Be reaction. We find that the direct-reaction mechanism is capable of accounting for the majority of the (p,d) cross section at very low energies. In addition, the direct-reaction model provides a simple explanation for the observed anisotropy in the differential cross section.

The most recent compilation of thermonuclear reaction rates [37] assumed $S(0)=16.4$ MeV b for each of the ^{9}Be(p,d)^{8}Be and the ^{9}Be(p,α)^{6}Li reactions. The previously reported experiment and analysis [11] estimated the sum of the $S(0)$ values for the two reactions to be 35^{+45}_{-15} MeV b, where the primary source of the error was the uncertainty in the contribution from the subthreshold state. Our analysis indicates that the presence of this level does not lead to an enhancement of the cross section at very low energies. Contributions from the direct-reaction mechanism [shown for the ^{9}Be(p,d)^{8}Be reaction in Fig. 11] give rise to a smoothly varying $S(E)$. In addition, any resonant contribution from distant levels will also give rise to a slowly varying S factor at very low energies. Thus, the S factors for the ^{9}Be(p,d)^{8}Be reaction can be expected to extrapolate smoothly from the lowest-energy measurements given in Ref. [11]. This assumption is consistent with the aforementioned values assumed in Ref. [37]. However, as a result of the experimental data and analysis presented here, the uncertainty is considerably smaller than reported in Ref. [11], and is estimated to be $\pm 20\%$. The ^{9}Be(p,α)^{6}Li reaction has a magnitude comparable to ^{9}Be(p,d)^{8}Be at astrophysical energies, and is well described by the previous R-matrix parametrization [11]. Thus the extrapolation of this cross section to lower energies should also be accurate within 20%. Consequently, the destruction of ^{9}Be in stellar interiors can be calculated with confidence in the nuclear cross sections. However, it must also be noted that other phenomena, such mixing processes within stars, must be understood before the depletion of the stable isotopes of lithium, beryllium, and boron can be completely understood [5].

Finally we note that the existing absolute cross section data for ^{9}Be(p,d)^{8}Be and ^{9}Be(p,α)^{6}Li at very low energies [11] have large errors (see, for example, Figs. 10 and 11). It appears practical with modern high-current accelerators to further reduce the uncertainty in the extrapolation by making additional precise absolute cross section measurements at energies below $E_p=100$ keV.

ACKNOWLEDGMENTS

The authors would like to thank Z. Ayer, B. J. Crowe, S. E. Hale, L. Ma, D. C. Powell, and M. H. Wood for their assistance in the data collection process. We also acknowledge useful discussions with G. M. Hale and A. J. Sierk. We would also like to thank B. Chaboyer for clarifying the roles of these reactions in the stellar depletion of beryllium. This work was supported in part by the U.S. Department of Energy, Office of High Energy and Nuclear Physics, under Grant Nos. DE-FG05-88ER40442 and DE-FG02-97ER41041.

[1] A. M. Boesgaard and J. R. King, Astron. J. **106**, 2309 (1993).
[2] F. Primas, D. K. Duncan, M. H. Pinsonneault, C. P. Deliyannis, and J. A. Thorburn, Astrophys. J. **480**, 784 (1997).
[3] N. Prantzos, M. Casse, and E. Vangioni-Flam, Astrophys. J. **403**, 630 (1993).
[4] B. Chaboyer, Astrophys. J. Lett. **432**, L47 (1994).
[5] C. P. Deliyannis, S. G. Ryan, T. C. Beers, and J. A. Thorburn, Astrophys. J. Lett. **425**, L21 (1994).
[6] C. J. Copi, D. N. Schramm, and M. S. Turner, Science **267**, 192 (1995).
[7] R. N. Boyd and T. Kajino, Astrophys. J. Lett. **336**, L55 (1989).
[8] D. Thomas, D. N. Schramm, K. A. Olive, G. J. Mathews, B. S. Meyer, and D. N. Fields, Astrophys. J. **430**, 291 (1994).
[9] A. J. Elwyn, J. E. Monahan, and J. P. Schiffer, Nucl. Fusion **11**, 551 (1971).
[10] J. R. McNally, Nucl. Fusion **11**, 554 (1971).
[11] A. J. Sierk and T. A. Tombrello, Nucl. Phys. **A210**, 341 (1973).
[12] T. B. Clegg, H. J. Karwowski, S. K. Lemieux, R. W. Sayer, E. R. Crosson, W. M. Hooke, C. R. Howell, H. W. Lewis, A. W. Lovette, H. J. Pfutzner, K. A. Sweeton, and W. S. Wilburn, Nucl. Instrum. Methods Phys. Res. A **357**, 200 (1995).
[13] T. C. Black, B. E. Hendrix, E. R. Crosson, K. A. Fletcher, H. J. Karwowski, and E. J. Ludwig, Nucl. Instrum. Methods Phys. Res. A **333**, 239 (1993).
[14] E. J. Ludwig, T. C. Black, C. R. Brune, W. H. Geist, and H. J. Karwowski, Nucl. Instrum. Methods Phys. Res. A **388**, 37 (1997).
[15] M. Uhrmacher, K. Pampus, F. J. Bergmeister, D. Purschke, and K. P. Lieb, Nucl. Instrum. Methods Phys. Res. B **9**, 234 (1985).
[16] C. R. Brune, H. J. Karwowski, and E. J. Ludwig, Nucl. Instrum. Methods Phys. Res. A **389**, 421 (1997).
[17] T. A. Welton, in *Fast Neutron Physics*, edited by J. B. Marion and J. L. Fowler (Interscience, New York, 1963), Vol. II, p. 1317.
[18] E. Jahnke and F. Emde, *Tables of Functions* (Dover, New York, 1943).
[19] V. Meyer, R. E. Pixley, and P. Truöl, Nucl. Phys. **A101**, 321 (1967).
[20] M. Balakrishnan, M. K. Mehta, and A. S. Divatia, Nuovo Cimento A **21**, 205 (1971).
[21] L. Bland and H. T. Fortune, Phys. Rev. C **21**, 11 (1980).
[22] F. C. Young, R. A. Lindgren, and W. Reichart, Nucl. Phys. **A176**, 289 (1971).

[23] A. Cichocki, J. Dubach, R. S. Hicks, G. A. Peterson, C. W. de Jager, H. de Vries, N. Kalantar-Nayestanaki, and T. Sato, Phys. Rev. C **51**, 2406 (1995).
[24] A. M. Lane and R. G. Thomas, Rev. Mod. Phys. **30**, 257 (1958).
[25] N. Kumar and F. C. Barker, Nucl. Phys. **A167**, 434 (1971).
[26] K. H. Bray, A. D. Frawley, T. R. Ophel, and F. C. Barker, Nucl. Phys. **A288**, 334 (1977).
[27] G. Raimann, B. Bach, K. Grün, H. Herndl, H. Oberhummer, S. Engstler, C. Rolfs, H. Abele, R. Neu, and G. Staudt, Phys. Lett. B **249**, 191 (1990).
[28] Y. Yamashita, Nucl. Phys. **A582**, 270 (1995).
[29] Y. Yamashita and Y. Kudo, Nucl. Phys. **A589**, 460 (1995).
[30] H. Herndl, H. Abele, G. Staudt, B. Bach, K. Grün, H. Scsribany, H. Oberhummer, and G. Raimann, Phys. Rev. C **44**, R952 (1991).
[31] F. D. Becchetti, C. A. Fields, R. S. Raymond, H. C. Bhang, and D. Overway, Phys. Rev. C **24**, 2401 (1981).
[32] R. Bass, *Nuclear Reactions with Heavy Ions* (Springer-Verlag, Berlin, 1980), pp. 180–188.
[33] M. H. Macfarlane and S. C. Pieper, Argonne National Laboratory Report No. ANL-76-11, Rev. 1 (unpublished), modified by R. P. Goddard, 1980.
[34] H. J. Votava, T. B. Clegg, E. J. Ludwig, and W. J. Thompson, Nucl. Phys. **A204**, 529 (1973).
[35] S. E. Darden, G. Murillo, and S. Sen, Nucl. Phys. **A266**, 29 (1976).
[36] R. V. Reid, Ann. Phys. (N.Y.) **50**, 411 (1968).
[37] G. R. Caughlin and W. A. Fowler, At. Data Nucl. Data Tables **40**, 283 (1988).
[38] B. Vaucher, J. C. Alder, and C. Joseph, Helv. Phys. Acta **43**, 237 (1970).
[39] R. de Swiniarski, F. G. Resmini, Ch. Glashausser, and A. D. Bacher, Helv. Phys. Acta **49**, 227 (1976).
[40] S. G. Buccino and A. B. Smith, Phys. Lett. **19**, 234 (1965).
[41] A. A. Fife, G. C. Neilson, and W. K. Dawson, Nucl. Phys. **A91**, 164 (1967).
[42] Y. S. Park, A. Niiler, and R. A. Lindgren, Phys. Rev. C **8**, 1557 (1973).
[43] P. D. Forsyth, A. R. Knudson, and F. C. Young, Nucl. Phys. **A85**, 153 (1966).
[44] These parameters are slightly different from those reported in Ref. [11], but are the parameters used to generate the curves reported in Ref. [11]. A. J. Sierk (private communication).